International Journal of Nanomedicine

Dovepress
Taylor & Francis Group

Open Access Full Text Article

ORIGINAL RESEARCH

Transplanted Iron Oxide Nanoparticle-Labeled Mesenchymal Stem Cells Exhibit ex vivo Neuronal Firing Activity in Ischemic Stroke Rats

Dong-Ming Huang[1], Chen-Wen Lu[2], Jong-Kai Hsiao[2,3]

[1]Institute of Biomedical Engineering and Nanomedicine, National Health Research Institutes, Miaoli, Taiwan; [2]Department of Medical Imaging, Taipei Tzu Chi Hospital, Buddhist Tzu Chi Medical Foundation, New Taipei City, Taiwan; [3]School of Medicine, Tzu Chi University, Hualien, Taiwan

Correspondence: Jong-Kai Hsiao, Department of Medical Imaging, Taipei Tzu Chi Hospital, Buddhist Tzu Chi Medical Foundation, No. 289, Jian Guo Road, Xindian District, New Taipei City, 23142, Taiwan, Tel +886-2-6628-9779-61714, Fax +886-2-86272976, Email jongkai@tzuchi.com.tw

Purpose: Mesenchymal stem cell (MSC) therapy shows promise in preclinical ischemic stroke models, yet clinical translation remains inconsistent. To address this gap, we investigated whether labeling MSCs with Ferucarbotran enables magnetic resonance imaging (MRI) tracking and enhances neural differentiation and functional integration, particularly focusing on the novel observation of spontaneous neuronal firing activity in transplanted cells.

Methods: Rat MSCs (rMSCs) were transduced with red fluorescent protein (RFP) and labeled with Ferucarbotran to generate Fer-RFP$^+$ rMSCs. These were transplanted into rats subjected to middle cerebral artery occlusion. MRI tracked cell migration and localization. Behavioral recovery was evaluated via the corner test, modified neurological severity score (mNSS), and infarct volume analysis. Post-transplantation, Fer-RFP$^+$ rMSCs were magnetically isolated for ex vivo electrophysiological and immunocytochemical analyses.

Results: Ferucarbotran labeling did not impair rMSC viability and enhanced in vitro proliferation. MRI effectively visualized Fer-RFP$^+$ rMSC migration to ischemic regions. Rats receiving Fer-RFP$^+$ rMSCs showed significantly improved functional recovery and reduced infarct volumes compared to controls. Remarkably, ex vivo isolated Fer-RFP$^+$ rMSCs exhibited spontaneous neuronal firing on multi-electrode array recordings and expressed the neuronal marker NeuN.

Conclusion: Ferucarbotran-labeled MSCs not only serve as MRI-visible tracers but also exhibit neuronal electrophysiological properties post-transplantation in an ischemic stroke model. The emergence of spontaneous neuronal firing in ex vivo transplanted MSCs suggests functional neuronal differentiation, potentially underpinning the observed therapeutic effects. These findings offer new mechanistic insights into MSC-mediated stroke recovery and may enhance the translational relevance of MSC-based therapies.

Keywords: mesenchymal stem cells, iron oxide nanoparticles, ischemic stroke, magnetic resonance imaging, neural differentiation, neuronal firing activity

Introduction

Stroke is the most common cause of disability and the second leading cause of death worldwide.[1] Unfortunately, due to population aging and limited therapeutic options for functional recovery, stroke incidence and its related burden are expected to increase.[2,3] In the past decade, stem cell therapy has emerged as a novel and promising approach to treat stroke and other neurological disorders because of stem cells' capacity for self-renewal, homing, and multilineage differentiation.[4–6] Particularly, transplantation of mesenchymal stem cells (MSCs) has been extensively studied for the treatment of stroke due to these properties as well as their immunomodulatory effects, ease of isolation and rapid expansion, and potential for autologous use.[7–9]

Preclinical animal studies have demonstrated that MSC therapy can promote brain functional recovery after stroke, showing improvements in neurological function and reduction in infarct size.[10–13] However, despite these promising results in animal models, the therapeutic benefits of MSCs have not been consistently replicated in clinical trials.[14,15]

Received: 25 February 2025
Accepted: 15 August 2025
Published: 28 August 2025

Factors contributing to this discrepancy may include differences in study design, cell dose and administration route, patient selection, timing of transplantation, and the complex pathophysiology of human stroke compared to animal models.[11,12] These challenges highlight the need for a better understanding of the mechanisms underlying MSC therapy and for developing methods to enhance their therapeutic efficacy in clinical settings.

Therefore, tracking the fate of transplanted stem cells and elucidating their functional integration within the host tissue are critical steps toward optimizing MSC-based treatment of stroke. Magnetic resonance imaging (MRI) is one of the most powerful tools for tracking the fate of transplanted stem cells in vivo owing to its noninvasive nature, high spatial resolution, deep tissue penetration, and lack of irradiation. For cellular MRI, biocompatible contrast agents are required to effectively label stem cells in vitro. Currently, iron oxide nanoparticles (IONs) are among the most commonly used probes to monitor and track stem cells using MRI.[16] Moreover, in vivo real-time tracking of stem cells labeled with IONs in ischemic stroke has been reported.[17,18] However, in vivo MRI primarily provides information on cell location, migration, and distribution rather than on cell viability and differentiation of ION-labeled MSCs in diseased animal models,[19–21] including ischemic stroke.[22] Therefore, postmortem histological examinations are often necessary to determine the actual fate of transplanted MSCs in brain tissues.

The potential mechanisms underlying the therapeutic benefits of MSCs in stroke models have been extensively investigated, such as differentiation for cell replacement, immune modulation, secretion of neurotrophic factors, or promotion of angiogenesis and endogenous neurogenesis.[10,23] Initially, the ability of MSCs to differentiate into brain cells for cell replacement was supposed to be the main contributor to the therapeutic effect in stroke recovery.[9,10] However, growing studies do not support this concept.[5,23,24] Since only a small fraction of transplanted MSCs can survive and engraft in the ischemic area, and few MSCs show positivity for neural cell markers,[25,26] the replacement of damaged brain tissues involves complex processes not likely solved by the differentiation of MSCs into brain cells. Moreover, in vitro differentiation of MSCs into neural lineages cannot be confirmed by in vivo evidence;[11] therefore, little or no benefit is attributed to the replacement of functional neurons by trans-differentiated MSCs in vivo. The conflicting outcomes in MSCs' in vitro and in vivo differentiation propensities into neural lineages may be largely attributed to their heterogeneity and functional diversity, administration protocols, and animal conditions.[11,12,27] Therefore, alternative methods to determine the fate of transplanted MSCs are required to elucidate the mechanisms underlying MSC therapy for stroke, although studies have shifted focus from cell replacement by MSCs toward their bystander effects.[28]

Ferucarbotran (Bayer, Leverkusen, Germany), one of the few IONs approved by the Food and Drug Administration (FDA) for clinical applications, has a simple protocol to label human MSCs (hMSCs) without a transfecting agent and has been demonstrated to track hMSCs by MRI in vitro and in vivo.[29–31] Moreover, Ferucarbotran-labeled MSCs can still exert osteogenesis, adipogenesis, chondrogenesis, and, importantly, neurogenesis.[32] A recent study showed that MRI revealed the migration of Ferucarbotran-labeled rat MSCs (rMSCs) in a cell-based therapy model of ischemic stroke.[33] In this study, we used Ferucarbotran to label rMSCs or red fluorescent protein (RFP)-transduced rat MSCs (RFP^+ rMSCs) efficiently, rapidly, and safely. The effects of Ferucarbotran labeling on in vitro cellular MRI and cell attributes were performed to evaluate the transplantation applicability of Ferucarbotran-labeled rMSCs (Fer-rMSCs) to the cell-based therapeutic model of stroke. After transplantation of Ferucarbotran-labeled RFP^+ rMSCs (Fer-RFP^+ rMSCs) in a rat model of ischemic stroke, serial MRI was performed to track the distribution and migration of grafted cells, and their therapeutic effects were also assessed. Furthermore, the present study investigated the electrophysiological characteristics of transplanted Fer-RFP^+ MSCs isolated from brain tissues to determine the potential mechanisms of MSCs in ischemic stroke therapy.

Materials and Methods

Cell Culture

Rat mesenchymal stem cells (rMSCs) were isolated from the bone marrow of Sprague-Dawley rats. Briefly, femora and tibiae were aseptically removed from 4–6-week-old male rats, according to the Institutional Animal Care and Use Committee of Taipei Tzu Chi General Hospital (IACUC no. 105-IACUC-003). The bone marrows were flushed

out using Dulbecco's Modified Eagle's medium (DMEM; Thermo Fisher Scientific, Waltham, MA, USA), supplemented with 10% (v/v) FBS (Biological Industries, Cromwell, CT, USA), 100 U/mL penicillin, and 100 μg/mL streptomycin, and then centrifuged at 1500 rpm for 5 min. Thereafter, the collection was added with Ficoll-Paque (GE Healthcare, IL, USA) and centrifuged at 2400 rpm for 20 min to collect the cells. The middle layer of bone marrow cells was collected, added to DMEM medium, and centrifuged at 1500 rpm for 5 min. Cells were counted, and 1×10^6 bone marrow cells were cultured in a 10 cm culture dish at 37°C in a humidified atmosphere of 5% CO_2. After one day, the bone marrow cell culture medium was transferred to a new dish. The medium was replaced every 2–3 days. Red fluorescent protein (RFP)-transduced rat MSCs (RFP^+ rMSCs) were prepared as in our previous study.[33]

ION Labeling and Cellular Attributes

rMSCs or RFP^+ rMSCs were treated with Ferucarbotran (Resovist®, Bayer Pharma AG, Berlin, Germany) at 100 μg Fe/mL for cells seeded at 10^6 in a 10 cm^2 dish overnight in the culture medium. After incubation at 37°C in 5% CO_2 for 1 day or 7 days, unbound Ferucarbotran was removed with three washes of 1× phosphate-buffered saline (PBS). Ferucarbotran-labeled rMSCs (Fer-rMSCs) or RFP^+ rMSCs (Fer-RFP^+ rMSCs) were examined for their cell viability via the MTT assay, reactive oxygen species (ROS) induction, mitochondrial membrane potential (MMP) change, immunological marker expression, flow cytometric side scatter counts (SSC), Prussian blue (PB) staining, and in vitro MRI.

Cell Viability

After treatment with Ferucarbotran followed by washing, MTT dye was added at 0.5 mg/mL to the cells in the medium for 1-hour incubation. The purple formazan dye generated by viable cells was proportional to the number of viable cells and measured at 570 nm absorbance using a microplate reader (Infinite F200; TECAN, Austria).

ROS Determination

After Ferucarbotran labeling and washing, dichlorofluorescein diacetate (DCFDA) (Molecular Probes, Eugene, OR, USA) was added at 10 μM to the cells in the medium at 37°C in the dark for 30 min incubation. The cells were trypsinized and collected in cold PBS for flow cytometry analysis (Becton-Dickinson, PharMingen USA) with an excitation wavelength of 488 nm and an emission wavelength of 515 nm.

MMP Assay

Following Ferucarbotran labeling and washing, 3,3′-dihexyloxacarbocyanine iodide [$DiOC_6(3)$] (Sigma-Aldrich Co.) was added at 40 nM to the cells in the medium at 37°C in the dark for 30 min incubation. The cells were trypsinized and collected in cold PBS for flow cytometry analysis (Becton-Dickinson, PharMingen USA) with an excitation wavelength of 488 nm and an emission wavelength of 501 nm.

Immunological Examination

After Ferucarbotran labeling and washing, the cells were fixed in 4% paraformaldehyde (Sigma-Aldrich) solution in PBS at room temperature for 10 min and washed twice with PBS. The non-specific binding sites were blocked with 2% bovine serum albumin (BSA) solution at room temperature for 30 min. The cells were then incubated with CD34 (1:500, GeneTex, CA, USA), CD29 (1:200, BioLegend, San Diego, USA), and CD90 (1:200, BioLegend, San Diego, USA) antibodies at room temperature for 2 hours. The cells were washed and then incubated with secondary Alexa Fluor 488 (Thermo Fisher Scientific, MA, USA) or Alexa Fluor 647 (Thermo Fisher Scientific) antibodies at room temperature for 2 hours. The samples were washed again with PBS, followed by staining with the DNA-binding dye 4′,6-diamidino-2-phenylindole (DAPI; 5 μg/mL; Molecular Probes) in PBS at room temperature for 5 min. The cells were then washed twice and imaged using an inverted microscope (Eclipse TS100; Nikon, Tokyo, Japan).

Flow Cytometry SSC

The cells, labeled with Ferucarbotran or not, were washed, trypsinized, and collected in cold PBS for flow cytometry (FACSCalibur; BD Biosciences, Franklin Lakes, NJ, USA) and analyzed using CellQuest Pro software (Becton Dickinson, Mississauga, CA) to determine the cell number of SSC measurements.

PB Staining

After Ferucarbotran labeling and washing, the cells were washed and incubated with Prussian blue (Millipore) for 5 min before light microscopy observation (Nikon TE2000-S).

In vitro Cellular MRI

The Ferucarbotran-labeled cells were collected by trypsinization and then washed, centrifuged, and placed in 300-μL Eppendorf tubes (1×10^5 cells per tube) in a water tank. T2-rapid acquisition with relaxation enhancement (RARE) pulse sequences were used (TR/TE = 3000/12.276 ms, flip angle = 180°, matrix size = 256×256). The slice thickness was 1.0 mm with a 1.0-mm gap. The field of view (FOV) was 80×80 mm for coronal scanning of the test tubes and 10 minutes and 40 seconds for sagittal scanning at the NEX of 5. All images were then analyzed using the Import Bruker NMR Files and ImageJ software.

Brain Stroke Model and Cell Therapy

All animal procedures and protocols adhered to the regulations of the Animal Care and Use Committee at Taipei Tzu Chi Hospital. These procedures followed the guidelines for the care and use of laboratory animals (IACUC approval number: 105-IACUC-003). Experiments were carried out as previously described.[33] Male Sprague-Dawley rats, 6–8 weeks old, were shaved on the neck and disinfected with 70% alcohol. Incisions were made layer by layer through the skin, subcutaneous tissue, and muscles to expose the bilateral common carotid arteries. The rats were fixed on a stereotaxic frame. We removed the right orbital bone behind the eye to expose the right middle cerebral artery (MCA) and induced an MCA occlusion by ligating the right MCA with 10–0 nylon sutures. The bilateral common carotid arteries were also clamped for 90 minutes using surgical clips. After 90 minutes, the clamps on the common carotid arteries were released to induce reperfusion injury. One hour after the ischemia-reperfusion procedure, the cell treatment group received an injection of 1 × 10^6/10 μL Fer-RFP$^+$ rMSCs dissolved in 10% fetal bovine serum (FBS) into the left corpus callosum of the brain-injured rats. In the control group, 1 × 10^6/10 μL rMSCs dissolved in 10% FBS were injected into the right corpus callosum (coordinates: AP: 0 mm, ML: ±2.0 mm, DV: 3 mm).

In vivo MRI

Fer-RFP$^+$ rMSCs were visualized by MRI at the indicated times after MCA occlusion surgery. Rats were anesthetized with isoflurane, and T2 images were acquired using a 7T MRI system (Biospec 70/30; Bruker, Ettlingen, Germany) with the following parameters: repetition time/echo time = 5000/56 ms; resolution = 256×256 pixels; slice thickness = 5 mm; and field of view = 30×30 cm².

Brain PB Staining

Rat brains were collected at post-stroke day 35 and embedded in paraffin for sectioning at a thickness of 5 μm. After serial rehydration, sections were incubated with Prussian blue (Millipore) for 20 min and then counterstained with nuclear fast red (Millipore) for 5 min before light microscopy observation.

Transmission Electron Microscopy (TEM) Image

Rat brains slide were collected at post-stroke day 35 and cutting at a thickness of 0.3×0.3 cm and washed with phosphate-buffered saline (pH7.2) (PBS; Sigma-Aldrich Co)., Cells were fixed containing 2% paraformaldehyde (Sigma-Aldrich Co.) and 2.5% glutaraldehyde (Sigma-Aldrich Co.) in 0.2 M cacodylate (pH 7.4) (Sigma-Aldrich Co.) for 2.5 hours at 4 °C, After then incubated with 1% osmium tetroxide (OsO4) buffer for 2 hours in the dark for post-fixation, After

dehydration, rinsing and embedding. Slices were cut from the dried sections with a diamond knife and placed on the grids. Images were taken using a TEM with a CCD camera (Hitachi H-7100; Hitachi, Ibaraki, Japan).

Therapeutic Effects

An experienced investigator blinded to the experimental design evaluated the sensory and motor aspects of brain function and sensorimotor disability after ischemia–reperfusion injury using the Modified Neurological Severity Score (mNSS) assessment and the corner test, respectively, as previously described.[33] In the mNSS, the failures of ischemic rats in the walking, righting, placing, balance, and body resistance tests were assigned as follows: scores of 1–6 indicated mild injury, 7–12 moderate injury, and 13–18 severe injury, with a score of 18 indicating maximum disability. In the corner test, rats were positioned in front of two boards angled at 30°; when they walked into the corner, vibrissae stimulation was applied to direct them to turn or rear to one side (right or left). The loss of vibrissae sensation and left-side rearing disability due to right MCA occlusion made ischemic rats turn more frequently to the right side. A score of 7 indicated no neurologic deficit, whereas a score of 15 indicated severe sensorimotor disability.

Immunohistochemistry

Brain slices were fixed with 4% paraformaldehyde solution at room temperature for 24 hours. The paraffin was removed by 1× Trilogy (Cell Marque Corporation, Rocklin, CA, USA) for 10 min under a pressurized environment. The tissue slices were treated with 0.3% H_2O_2 for 30 min to eliminate endogenous peroxidase activity. Then, we washed the tissue slices with PBS and blocked them with 2% BSA for 60 min. The tissue slices were treated with primary antibodies, including anti-NESTIN antibody (1:250; Abcam, Cambridge, USA), rabbit anti-KI67 monoclonal antibody (1:150; GeneTex, CA, USA), recombinant anti-GFAP antibody (1:250; Abcam, Cambridge, USA), or mouse anti-NeuN monoclonal antibody (1:200; Millipore, MA, USA). Following this, the tissue slices were incubated with an SS IHC detection kit (BioGenex, San Ramon, CA, USA) containing biotinylated goat anti-mouse secondary antibody and horseradish peroxidase (HRP) enzyme for 30 min. After washing thrice with 1× PBS, color development was performed using Fast Red (Sigma, Temecula, USA). These antibodies were prepared by dilution with PBS containing 2% BSA at the proportions described above. The tissue slices were treated with primary antibodies overnight and then washed with PBS. Diaminobenzidine was then added for another 5 min, and the tissue slices were dehydrated via the ethanol gradient method and treated with xylene for 10 min. These tissue slices were mounted on Permount and visualized using an inverted light microscope (Eclipse TS80i; Nikon, Tokyo, Japan).

Isolation and Electrophysiological Characteristics of Fer-RFP$^+$ rMSCs

Rat brains were sectioned into 1-mm-thick coronal slices. Tissue samples were harvested from regions where rMSCs were detected by in vivo MRI, specifically the hipppocampus, caudate nucleus, and third ventricle. A tissue segment approximately 1 mm in diameter was transferred into 300-μL Eppendorf tubes and enzymatically digested using 0.75% collagenase II at 37°C with gentle rotation at 20 rpm for 1 hour. The samples were then centrifuged at 1500 rpm for 10 minutes at 4°C and washed three times with phosphate-buffered saline (PBS). For magnetic separation, a neodymium iron boron (NdFeB) magnet, with an approximate magnetic field strength of 5000 Gauss (data not shown), was positioned adjacent to the Eppendorf tubes containing the digested tissue. The NdFeB magnet used in this study was a commercially available product obtained from a local hardware store. Magnetic separation was performed for 1 hour, after which magnetically responsive cell pellets were collected and transferred into 6-well culture plates containing DMEM for further analysis.

We observed the growth of the separated tissue samples daily and after the re-expansion of the cells until 60–70% confluence, the cells were trypsinized, and 1×10^5 cells were seeded onto the MED probes (MED64 system, Alpha Med Science, MED-P545A) and incubated at 37°C in a 5% CO_2 atmosphere. After the cells grew to 70–80% confluence, multi-electrode recordings used a sampling rate of 50 kHz. The spike frequency was analyzed with a spike sorting analysis system.

Distribution and Survival of Fer-RFP$^+$ rMSCs

On the 37th day after brain calibration, the calibrated Fer-rMSCs in the brain slices were separated by the same method as above, and trypan blue was added to count the cell number and total number with an automatic cell counter (EVETM, Nano Entek, Koren).

Electrophysiological Characteristics of Fer-rMSCs, rMSCs, and Endothelial Cells

Ferucarbotran-labeled rMSCs (Fer-rMSCs) or unlabeled rMSCs (rMSCs) at 1×10^5 were directly seeded onto the MED probes (Alpha Med Science, MED-P545A) and incubated at 37°C in a 5% CO_2 atmosphere. The endothelial cells were isolated from the left cerebral cortex of the rMSC rat where rMSCs were previously injected into the right caudate nucleus. The rat was sacrificed, and a block of the left brain measuring 5 mm² was extracted without the assistance of a stereotaxic instrument. The cortex tissue was treated with 0.75% collagenase II at 37°C and rotated at 20 rpm for 1 hour. After collagenase digestion, the sample was centrifuged at 1500 rpm for 10 minutes at 4°C, washed three times with 1× PBS, and then placed in a 6-well plate for culture. We observed the growth of the cells daily, and when the cells were plated and grew properly, 1×10^3 cells were transferred to a culture dish in which 8×8 electrode grids were embedded. Once the cells reached 70–80% confluence, extracellular action potential signals and firing frequency were measured using the 64-channel multi-electrode array system (MED64, Diagnosys Sunpoint Scientific, Taiwan).

Statistical Analysis

Comparison between two groups was performed using *t*-tests. All statistical analyses were conducted using SigmaStat version 12.0 (Jandel Scientific, San Diego, CA). Data are expressed as the mean ± standard deviation (SD). Differences were considered significant as $*P < 0.05$, $**P < 0.01$, and $***P < 0.001$.

Results and Discussion

Cellular Attributes and Magnetic Labeling Efficiency

Although it is generally believed that IONs are biocompatible, the impacts of IONs on stem cell attributes remain an unresolved issue, which may be attributed to particle size, surface coating, iron concentration, incubation time, cell types, and experimental models. Ferucarbotran can be efficiently uptaken by stem cells for 1.5 T MRI detection and has several advantages such as good biocompatibility, low toxicity, and excellent stability.[29,30,32] However, cellular responses to Ferucarbotran labeling have been observed. Studies have shown that Ferucarbotran can promote the proliferation and migration of hMSCs toward cancers, suggesting that the impacts of Ferucarbotran on hMSCs are not necessarily harmful but favorable for cancer therapy.[34,35] Using Ferucarbotran labeling, studies of hMSCs revealed that it had no effects on neural differentiation and induced no changes in cellular functions, including morphology, viability, oxidative stress, and mitochondrial membrane energization.[32] These studies support the feasibility that the biocompatibility of Ferucarbotran is sufficient to label rMSCs for studying their therapeutic effects on ischemic stroke.[33]

First, in this study, the cellular viability effect of Ferucarbotran labeling was determined by the MTT assay. Interestingly, Ferucarbotran at 100 μg Fe/mL for 24-hour incubation induced significantly greater MTT increase in rMSCs, suggesting that Ferucarbotran is not cytotoxic but can activate the cellular activity of rMSCs (Figure 1A). This in vitro result was similar to previous studies in which Ferucarbotran promoted the growth of hMSCs,[35] which may benefit MSCs' therapeutic effects on stroke. Therefore, it is worth determining whether Ferucarbotran can stimulate the proliferation of MSCs in vivo.

After the internalization of IONs into cells, it is believed that free iron will be released into the cytoplasm due to the lysosomal degradation of IONs because they can be transferred into lysosomes,[35,36] which can possibly induce the generation of ROS through Haber-Weiss-Fenton reactions.[36] Moreover, MMP change is an early event for cell apoptosis and is highly correlated with ROS production.[37,38] Neither ROS induction (Figure 1B) nor MMP change (Figure 1C) was observed at day 1 or day 7 after Ferucarbotran incubation for 24 hours at 100 μg Fe/mL, which is similar to previous results obtained from hMSCs with Ferucarbotran labeling.[32] Moreover, to exclude possible adverse effects of Ferucarbotran on cellular functions, we examined the immunophenotypes or stemness of labeled rMSCs.

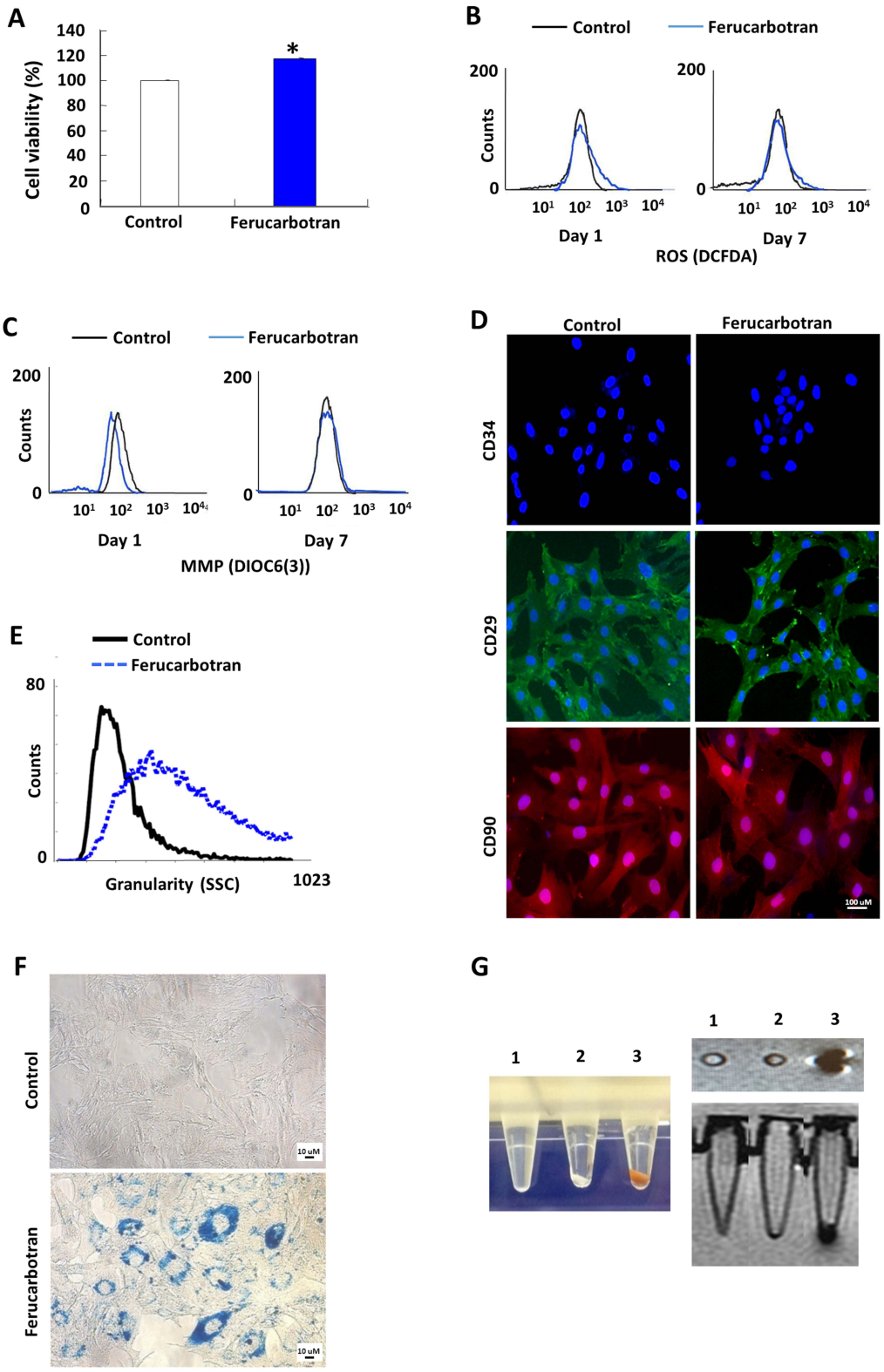

Figure 1 Cell attributes and in vitro cellular labeling. (**A**) Cell viability MTT assay. Ferucarbotran induced significantly greater MTT increase on rMSCs. (**B**) ROS production assay. No ROS induction was observed. (**C**) MMP alteration assay. No MMP change was induced by Ferucarbotran. (**D**) Cell surface marker expression. Ferucarbotran did not affect the expression of cell surface marker, CD34 (negative for MSCs), CD29 and CD90 (both positive for MSCs). (**E**) SSC based on flow cytometry. We observed significantly increased SSC in flow cytometry, indicating increased granularity in Ferucarbotran-labelled cells. (**F**) PB staining showed the internalization of Ferucarbotran as blue and black dots. (**G**) Color images of Ferucarbotran-labeled cell pellet (left panel). In vitro MRI demonstrated the labelling efficiency of Ferucarbotran (right panel). Tube 1: empty; tube 2: control cell pellet; tube 3: Ferucarbotran-labeled cell pellet.

https://doi.org/10.2147/IJN.S518933

Immunophenotypic characterization of rMSCs by immunofluorescent microscopy revealed that rMSCs were positive for CD29 and CD90 but negative for CD34. Identical immunophenotypic profiles were observed in Fer-rMSCs or control rMSCs (Figure 1D), suggesting Ferucarbotran did not affect the potential for differentiation in rMSCs. The above results indicated no noticeable unfavorable effects of Ferucarbotran labeling, which showed the biosafety of the Ferucarbotran labeling protocol for the following magnetic monitoring of rMSCs in vitro.

Using flow cytometric SSC analysis, Fer-rMSCs showed higher granularity compared to control rMSCs (Figure 1E), suggesting the efficient internalization of Ferucarbotran. Indeed, Prussian blue (PB) staining demonstrated the cellular internalization of IONs stained as blue granules in the cytoplasm (Figure 1F). The pellet of Fer-rMSCs displayed a brownish color (Figure 1G, left panel); moreover, under T2-weighted imaging mode, the MR image of Fer-rMSCs' pellet in the test tube placed in a water bath showed an obvious hypointense signal (Figure 1G, right panel). The efficient labeling and marked contrast effect in cellular MRI suggested the potential of Ferucarbotran labeling for detailed MRI in vivo.

In vivo MRI of Fer-RFP$^+$ rMSCs and Ischemic Brain

Because ischemic brain tissues display intrinsic bright positive signals in T2-weighted images in vivo,[33] IONs with hypointense signals are suitable to distinguish labeled MSCs in ischemic stroke sites. To assess the dynamic distribution of rMSCs in the stroke brain, Fer-RFP$^+$ rMSCs were injected into the left corpus callosum (CC) 1 hour after reperfusion in the right cerebral acute ischemic infarct model using MCAO. As shown in Figure 2A, the infarcted area appeared as hyperintense signals (white arrow) in the right brain, whereas the injection sites of Fer-RFP$^+$ rMSCs showed obvious hypointense signals corresponding to ION signals (blue arrowhead). Moreover, the ION signals could be detected in the ipsilateral lateral ventricle (red arrowhead 1), the contralateral lateral ventricle (red arrowhead 2), and even the infarcted area (red arrowhead 3). Serial MRI demonstrated the migration of Fer-RFP$^+$ rMSCs from day 1 to day 15 post-MCAO. By day 22 and day 36, the extent of visible migration had diminished, although Fer-RFP$^+$ rMSCs remained detectable These observations suggest an initial phase of active migration followed by reduced motility over time, indicating potential long-distance migration and early engraftment within the infarct region. Histological PB staining and Transmission electron microscopy (TEM, Figure 2C) of ION hypointense signal-positive areas—ipsilateral lateral ventricle (top panel, Figure 2B), contralateral lateral ventricle (middle panel, Figure 2B), and infarcted area (bottom panel, Figure 2B)—also confirmed the wide distributions of IONs, which may support the relocation of Fer-RFP$^+$ rMSCs in the brain. In the present study, MRI successfully determined the dynamic distribution of ION-labeled MSCs in the stroke model.

Native MSCs can migrate, after they are exogenously delivered into animals, toward disease sites. Ferucarbotran can not only monitor the locations of MSCs in vivo but also improve the migration/homing capacities of hMSCs to cancers.[34] Additionally, dextran-coated IONs have been shown to promote the migration capacity of hMSCs toward lesioned dopaminergic neurons in a 6-hydroxydopamine (6-OHDA)-induced Parkinson's disease model in mice.[39] Although it is important to further examine whether Ferucarbotran can promote MSCs' migration toward the infarcted area, the relocation of Fer-RFP$^+$ rMSCs in this study may partly be attributed to Ferucarbotran-promoted MSCs' migration. The prerequisite for whether MSCs transdifferentiate or produce neurotrophic factors to replace or rescue damaged brain cells is their migration toward the ischemic stroke sites. The present results suggest that IONs, especially Ferucarbotran or alternative dextran-coated IONs, can not only be useful for tracking the fate of transplanted MSCs but also improve MSCs' therapeutics for ischemic stroke as well as other diseases. As mentioned above, it is critical to develop methods to determine MSCs' viability in vivo because our results (Figure 1A) and previous studies[34,35] have shown that Ferucarbotran labeling enhances MSC proliferation by suppressing H_2O_2-induced oxidative stress and promoting cell cycle progression. These effects may contribute to the therapeutic benefit of MSCs, possibly by augmenting their paracrine activity, including neurotrophic factor secretion. However, MRI seems possible but not yet successful in reflecting the tendency of cell viability in vivo.[22] TEM analysis of brain sections revealed that cells containing Ferucarbotran exhibited an active euchromatic nucleus without evidence of phagocytosed debris or immune granules, thereby supporting that the hypointense MRI signals originated from viable Fer-RFP$^+$ rMSCs rather than from host microglia or macrophages.

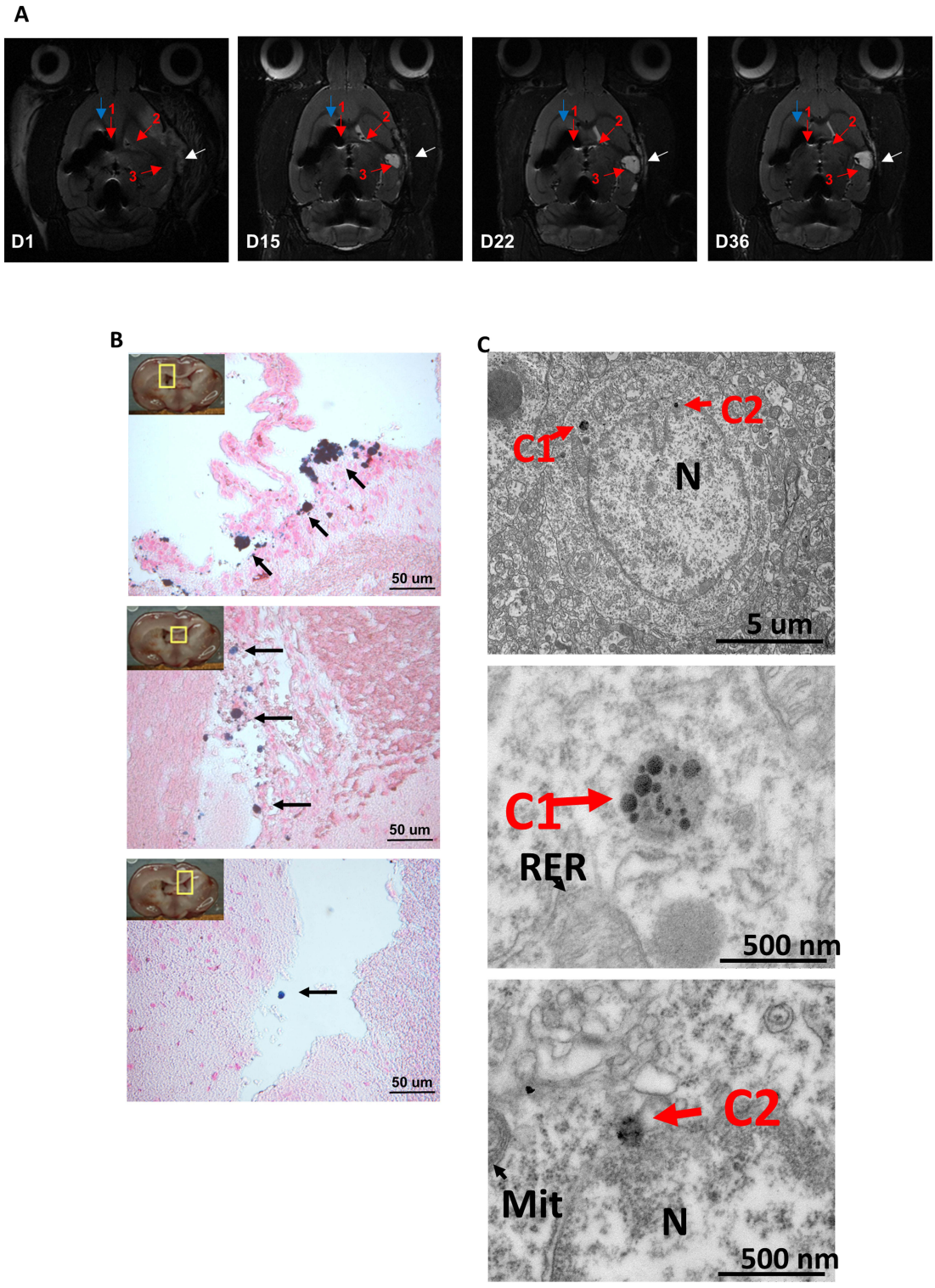

Figure 2 Localization and migration of Fer-RFP+rMSCs in stroke brain detected by serial MRI and PB staining. (**A**) Fer-RFP+rMSCs were located at the injection site (blue arrowhead), the ipsilateral lateral ventricle (red arrowhead 1), the contralateral lateral ventricle (red arrowhead 2) and the infarcted area (red arrowhead 3) under MRI scans at poststroke day 1, day 15, day 22 and day 36. The infarcted area was indicated as hyperintense signals (white arrowhead). (**B**) PB staining of specific regions (ipsilateral lateral ventricle, top panel; contralateral lateral ventricle, middle panel; infarcted area, bottom panel). The migration of Fer-RFP+rMSCs was observed. (**C**) TEM image Transmission electron microscopy (TEM) was used to observe ingested iron oxide nanoparticles (IONs) within brain injury tissue. C1, C2: The images show iron oxide nanoparticles (IONs; Resovist, ferucarbotran). TEM micrographs depict brain injury tissue labeled with iron oxide nanoparticles (IONs, 45–60 nm) coated with carboxydextran, marking rat bone marrow-derived mesenchymal stem cells (Pr-BM-rMSCs). Scale bars are set at 5 μm and 500 nm, respectively.

https://doi.org/10.2147/IJN.S518933

Therapeutic Effects

Certainly, MRI is a well-suited approach to the detection and identification of cell distribution and migration with high-resolution images. Because of intrinsic bright positive signals displayed by ischemic brain tissues, MRI is supposed to be able to evaluate the therapeutic effects of MSCs by detecting the infarct volumes appearing as hyperintense signals, as shown in Figure 3A–C. The infarct volume showed a rapid decline in the first 8 days after ischemic operation but then rebounded with a slow increase in the animals treated with saline (Control, white arrowhead, Figure 3A and D), suggesting short-term recovery of operation-induced edema and then sustained ischemic injury. A rapid and short-term recovery of infarct volume was also observed in the animals grafted with Fer-RFP$^+$ rMSCs in the contralateral corpus callosum (CC)(white arrowhead, Figure 3B and D) or unlabeled rMSCs in the ipsilateral corpus callosum (CC) (white arrowhead, Figure 3C and D); however, the infarct volumes in animals grafted with Fer-RFP$^+$ rMSCs and unlabeled rMSCs, after the first 8 days, still displayed a slow and long-term decline, suggesting the therapeutic effects of both grafted rMSCs. There were significantly lower infarct volumes in animals grafted with unlabeled rMSCs in the ipsilateral CC than in animals treated with saline at days 8, 15, and 29 after transplantation, but the infarct volumes in animals grafted with Fer-RFP$^+$ rMSCs in the contralateral CC were lower than in animals treated with saline just at days 15 and 29 after transplantation (Figure 3D). Moreover, significantly lower infarct volumes in animals grafted with unlabeled rMSCs in the ipsilateral CC than in animals grafted with Fer-RFP$^+$ rMSCs in the contralateral CC were observed at days 8, 15, and 29 after transplantation (Figure 3D), indicating a better therapeutic impact of rMSCs in the ipsilateral CC than Fer-RFP$^+$ rMSCs in the contralateral CC.

Neurological functions gradually recovered over time, with improvements in mNSS and corner test scores, in all three groups (Figure 3E). Both corner test and mNSS scores were significantly lower in animals grafted with Fer-RFP$^+$ rMSCs in the contralateral CC or grafted with unlabeled rMSCs in the ipsilateral CC than in animals treated with saline at days 7, 14, and 28 after transplantation. However, no significant differences were found between animals grafted with Fer-RFP$^+$ rMSCs in the contralateral CC and unlabeled rMSCs in the ipsilateral CC at each time point in either corner test or mNSS scores.

In this study, both transplantations of Fer-RFP$^+$ rMSCs in the contralateral CC and unlabeled rMSCs in the ipsilateral CC offered therapeutic benefits on stroke determined by the hyperintense signal of the infarction area and animal behavior tests. However, the transplantation of unlabeled rMSCs in the ipsilateral CC showed a better therapeutic outcome than the transplantation of Fer-RFP$^+$ rMSCs in the contralateral CC in infarction area MRI but not in corner test or mNSS scores. The correlation between infarction area MRI and animal behavior tests needs to be established. After the transplantation of Fer-RFP$^+$ rMSCs in the contralateral CC, these cells need to migrate and reach or get close to the infarct area; by contrast, unlabeled rMSCs will always be located on the infarct area. Supposedly, a smaller amount of MSCs can benefit MSCs' therapeutic outcome in animals grafted with Fer-RFP$^+$ rMSCs in the contralateral CC than in animals grafted with unlabeled rMSCs in the ipsilateral CC. However, as mentioned above, Ferucarbotran may positively alter MSCs' attributes such as proliferation and migration, and then improve MSCs' therapeutic outcome in stroke. It is vital to comprehensively evaluate the impacts of Ferucarbotran labeling on MSCs' fates after transplantation.

Neurologic Differentiation

MSCs' therapeutic benefits to stroke are not limited to their differentiation capacity to replace damaged neural cells but also extend to the bystander effects of secreted factors from MSCs. Regardless of the mechanisms responsible for MSC-mediated functional recovery in ischemic stroke, either neurogenesis or neurotrophic support is fundamental to the therapeutic application of MSCs in stroke. Compared with control animals, histological analysis of the infarct area showed much higher Ki67 expression in animals grafted with Fer-RFP$^+$ rMSCs in the contralateral CC and animals grafted with unlabeled rMSCs in the ipsilateral CC (Figure 4), suggesting that both Fer-RFP$^+$ rMSCs and rMSCs were highly proliferative after transplantation or that an activated proliferation of host cells was induced in infarct animals by either Fer-RFP$^+$ rMSCs or rMSCs. Interestingly, dramatic GFAP expression was also found in the infarct area of animals grafted with Fer-RFP$^+$ rMSCs in the contralateral CC and unlabeled rMSCs in the ipsilateral CC (Figure 4), indicating that vigorous astrogliosis was activated by either Fer-RFP$^+$ rMSCs or rMSCs. The reactive astrogliosis may be derived

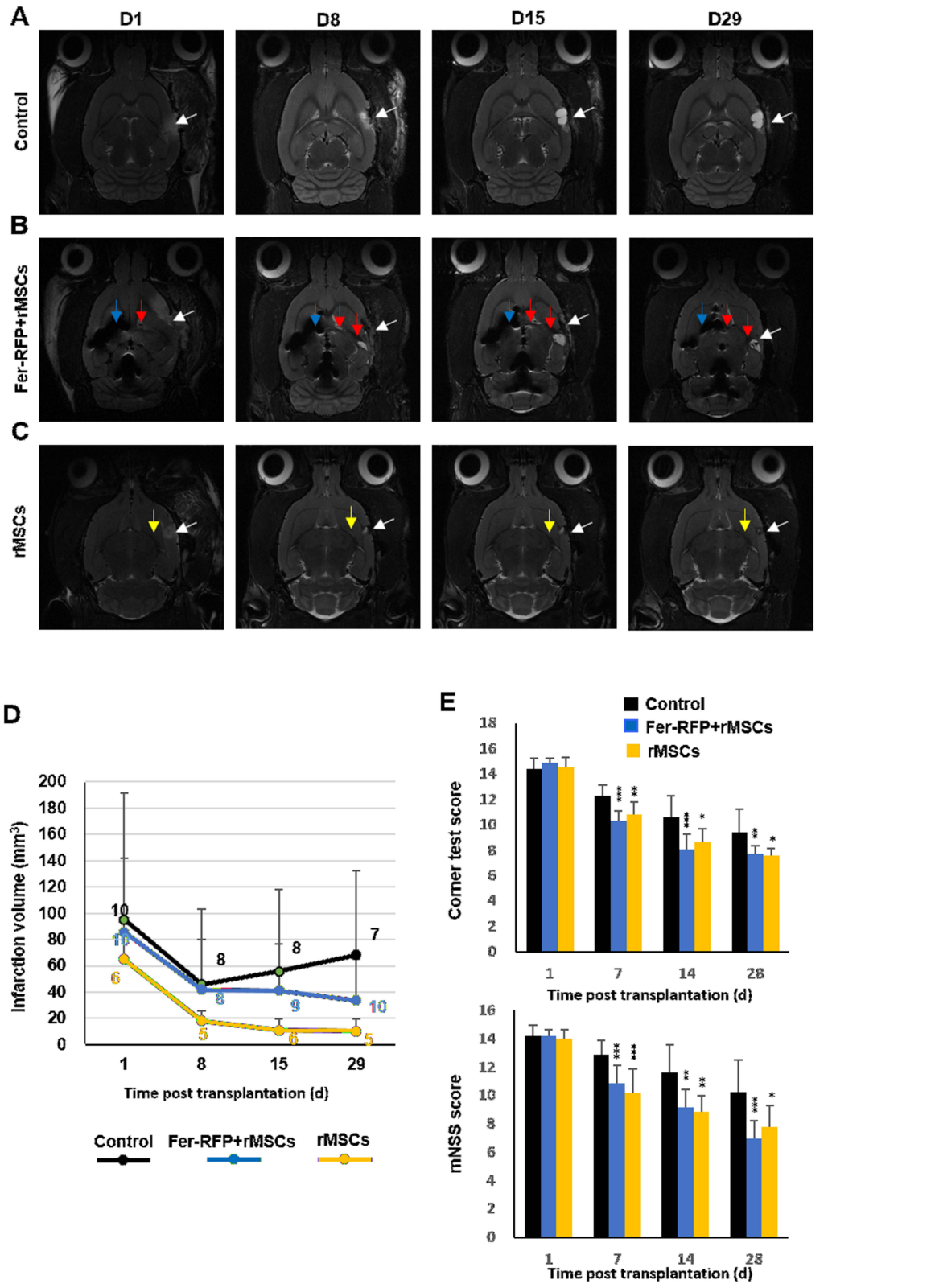

Figure 3 Therapeutic effects of transplanted rMSCs. (**A**–**C**) Representative sequential MRI images of stroke rats injected with (**A**) saline (control), (**B**) Fer-RFP$^+$ rMSCs, and (**C**) unlabeled rMSCs on days 1, 8, 15, and 29 post-transplantation. The infarct area appears hyperintense (white arrowheads). Blue arrowheads indicate the injection site of Fer-RFP$^+$ rMSCs, and red arrowheads show the distribution toward the infarct region. Yellow arrowheads in panel C indicate the rMSC injection site. (**D**) Infarct volume measured over time, showing reduced lesion size in the rMSC-treated group. (**E**) Behavioral analysis: upper graph shows corner test scores, and lower graph shows modified neurological severity scores (mNSS) at various time points post-transplantation. Data are presented as mean ± standard deviation (*p < 0.05; **p < 0.01; ***p < 0.001).

https://doi.org/10.2147/IJN.S518933

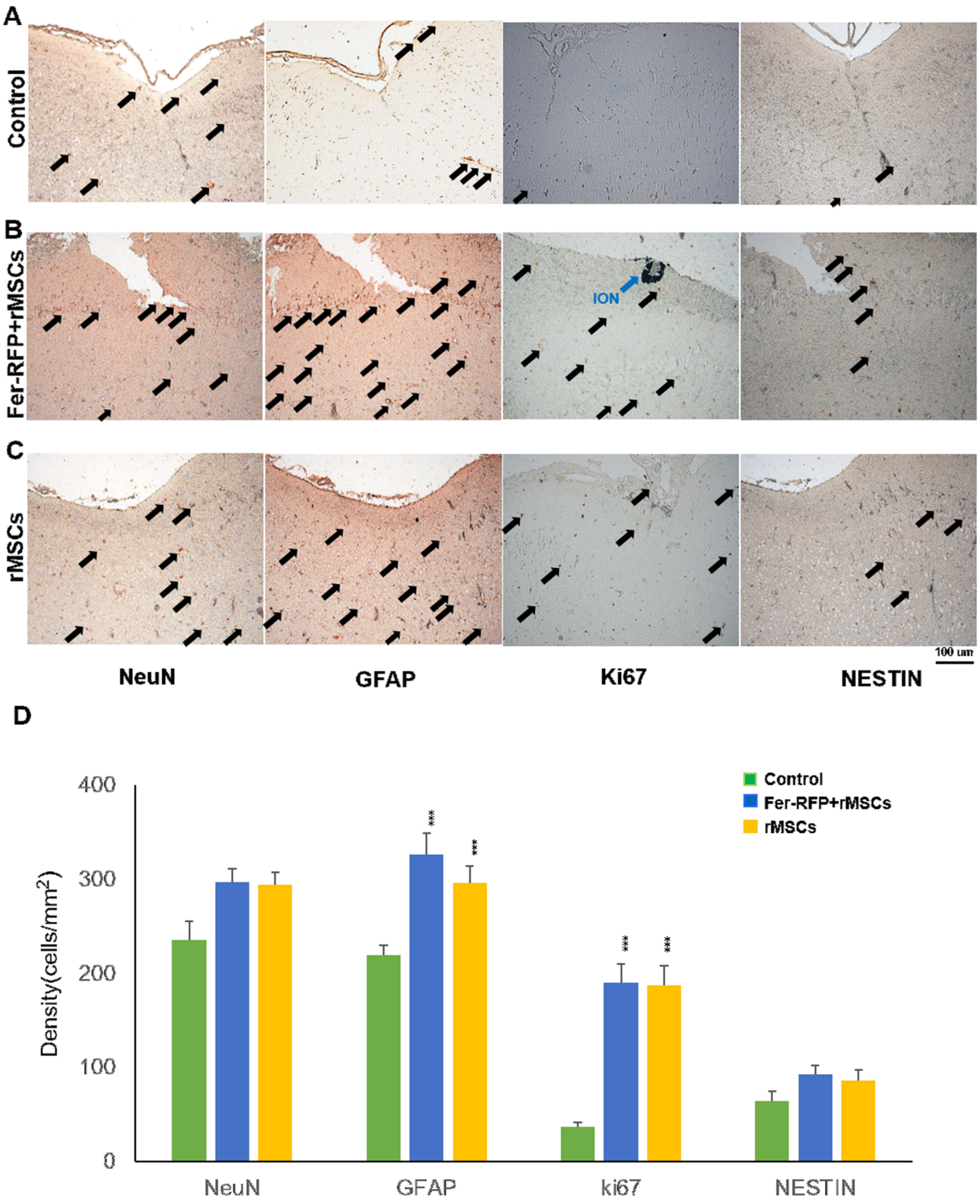

Figure 4 Histological examination of neural differentiation and proliferating markers (NeuN, GFAP, Ki67 and NESTIN) in the infarct area of animals grafted with saline (**A**), Fer-RFP+rMSCs (**B**), and unlabeled rMSCs (**C**). (**D**) The quantification of marker expression, control and treatment groups. Data are presented as mean ± standard deviation.(***: $p < 0.001$).

from the differentiation of either Fer-RFP$^+$ rMSCs or rMSCs or could alternatively be attributed to the intrinsic astroglial activation mediated by Fer-RFP$^+$ rMSCs or rMSCs. Although increased cell proliferation is thought to contribute to reactive astrogliosis, only modest and statistically non-significant differences were observed in NeuN and NESTIN expression among groups (NeuN: Control vs Fer-RFP$^+$ rMSCs, P = 0.0641; Control vs rMSCs, P = 0.0712; NESTIN: Control vs Fer-RFP$^+$ rMSCs, P = 0.0323; Control vs rMSCs, P = 0.1012), suggesting that neurogenesis was not markedly induced despite the proliferative environment in the infarcted region following transplantation. Our results suggest the possibility that Fer-RFP$^+$ rMSCs or rMSCs had a high ability to differentiate into glial cells but not neurons. Moreover, it was more likely that the bystander effects of Fer-RFP$^+$ rMSCs or rMSCs were the main contributors to the therapeutic benefits rather than direct cell replacement. No differences in cell proliferation and astrogliosis induction between animals grafted with Fer-RFP$^+$ rMSCs in the contralateral CC and animals grafted with unlabeled rMSCs in the ipsilateral CC highlight that Ferucarbotran may have significant and positive impacts on MSCs' attributes, including, but not limited to, the differentiation of themselves and their bystander effects to improve the therapeutic benefits of MSCs in stroke.

Electrophysiological Function

After MSC transplantation and migration toward the infarct area in stroke, they must maintain their viability, differentiation capacity, and other properties and functions for a long time. Although histological examination can provide end-point information about MSCs' fate, technical issues such as immunological co-staining of cell contamination still exist, potentially misestimating MSCs' attributes. Studies, including the present report, have shown the successful tracking of MSCs' migration and distribution using MRI with cellular labeling of IONs; however, the inability to dynamically detect the above-mentioned attributes of MSCs is a major obstacle to their approval for clinical use. Notably, cell labels must not interfere with any of MSCs' attributes. IONs are currently the only inorganic nanomaterial approved by the FDA for medical uses. It is also accepted that IONs are extremely biocompatible and degraded through normal iron metabolism in the body. However, recent studies as well as the present study have shown that IONs can not only track MSCs but also affect cell attributes, including migration, proliferation, and differentiation,[34,35,39] suggesting that IONs can instead multifunctionally benefit MSCs' attributes for therapy in stroke.

As mentioned above, because no sufficiently differentiated and functional neurons from MSCs were observed in vivo, the emphasis on MSCs' differentiation for cell replacement in stroke recovery has shifted toward their bystander effects. However, we wondered whether IONs may benefit MSCs' differentiation. In addition to stem cell tracking, IONs have been successfully used in biomedical applications for magnetic cell delivery and separation.[40–42] To our knowledge, no studies about the features of ION-labeled MSCs recovered from brains after their transplantation have been reported. Therefore, after animals grafted with Fer-RFP$^+$ rMSCs were sacrificed, transplanted Fer-RFP$^+$ rMSCs were recovered from the indicated locations using magnetic attraction and then re-cultured in vitro (Figure 5A), as described in the Material and Methods. After long-term cell expansion, the differentiation of Fer-RFP$^+$ rMSCs to neuronal cells was determined by their electrophysiological characteristics using a multi-electrode recording MED64 system.

Surprisingly, transplanted Fer-RFP$^+$ rMSCs from the ipsilateral lateral ventricle underneath the injection sites spontaneously generated firing activity patterns in the MED64 chip, as shown in the middle panel of the left column in Figure 5B. Fer-RFP$^+$ rMSCs near channel 22 (top-left panel) or channel 31 (bottom-right panel) displayed significant but quite different action potentials in spike frequency and amplitude; however, no significant spontaneous firing activity patterns were observed in Fer-RFP$^+$ rMSCs near channel 23 (top-right panel) or channel 30 (bottom-left panel). Such heterogeneous expression of firing activity patterns of Fer-RFP$^+$ rMSCs may be attributed to many factors such as the heterogeneity of rMSCs.[43] Interestingly, regardless of whether Fer-RFP$^+$ rMSCs could generate spontaneous firing activity patterns, they were positively stained for NeuN expression, as shown in the right column in Figure 5B. Moreover, from a different animal, transplanted Fer-RFP$^+$ rMSCs could be isolated from the third ventricle and stained for positive RFP expression, confirming the long-distance migration of Fer-RFP$^+$ rMSCs in Figure 2B, and then these isolated Fer-RFP$^+$ rMSCs displayed highly firing activity patterns in a distinct MED64 (Figure 5C). The highly heterogeneous expression of firing activity patterns of Fer-RFP$^+$ rMSCs was also observed.

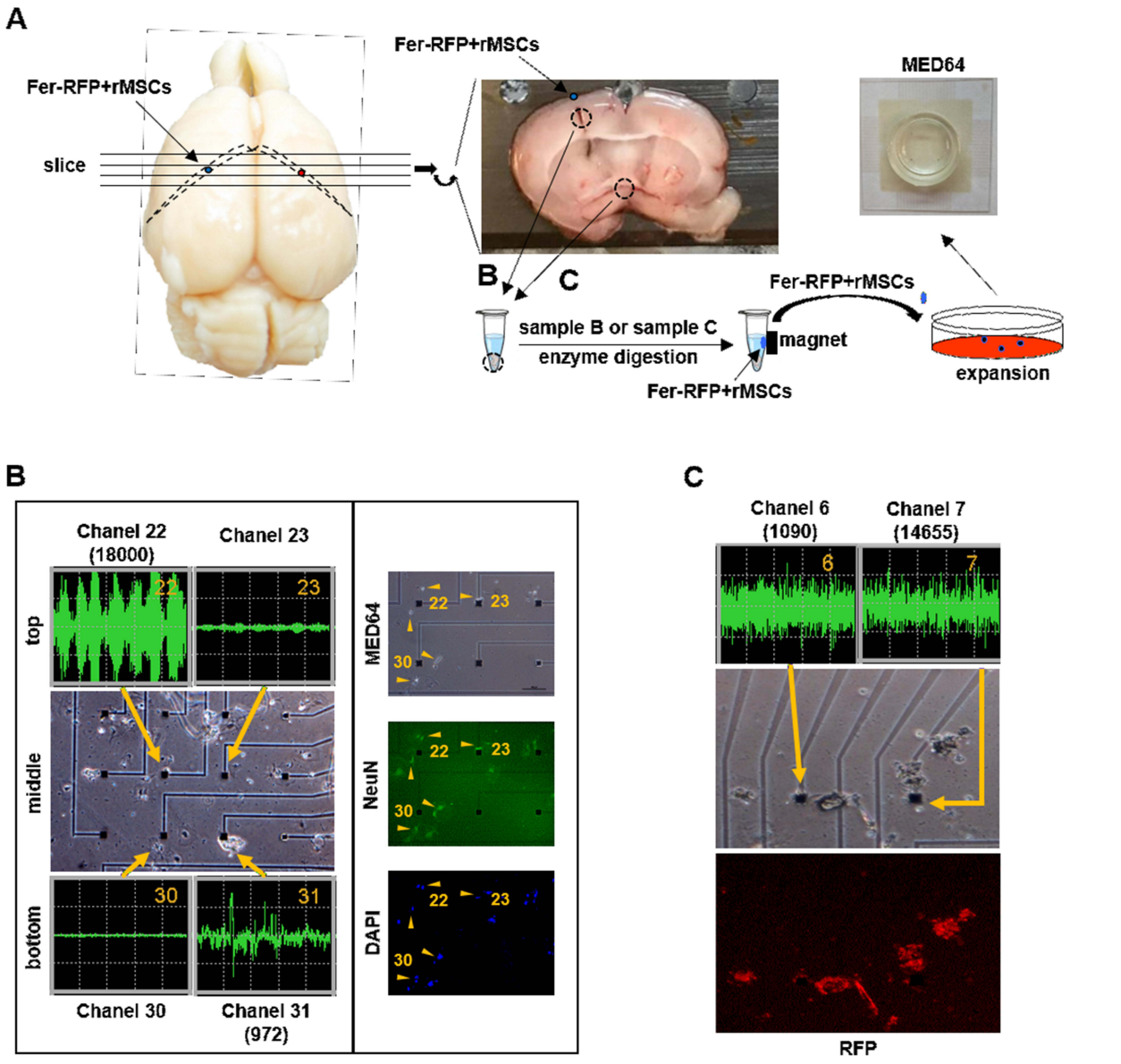

Figure 5 The isolation and electrophysiological characteristics of transplanted Fer-RFP+rMSCs. (**A**) The isolation process of transplanted Fer-RFP+rMSCs. (**B**) Left column, action potentials of transplanted Fer-RFP+rMSCs isolated from the ipsilateral lateral ventricle; right column, Fer-RFP+rMSCs were observed on MED64 and stained with NeuN antibody and DAPI. (**C**) Transplanted Fer-RFP+rMSCs isolated from third ventricle were examined for action potentials and observed for positive RFP. (**D**) Fer-rMSCs, rMSCs, or endothelial cells isolated from animals grafted with Fer-RFP+rMSCs did not display action potential.

However, without transplantation into rat brain, neither rMSCs nor Fer-rMSCs cultured solely in vitro could spontaneously generate firing activity patterns (Figure 5D), suggesting that Ferucarbotran could not induce non-transplanted rMSCs' neuronal differentiation ability. In addition, endothelial cells isolated from animals grafted with Fer-RFP$^+$ rMSCs could not spontaneously generate firing activity patterns (Figure 5D). Although no obvious evidence demonstrated the contribution of in vivo neuronal differentiation of Fer-RFP$^+$ rMSCs to stroke recovery, the results strongly suggest that Fer-RFP$^+$ rMSCs might acquire the ability of neuronal differentiation with functional activity via transplantation in stroke animals. Although it is difficult to isolate rMSCs without Ferucarbotran labeling after their transplantation from animals, it still needs further examination whether unlabeled rMSCs may spontaneously generate firing activity patterns as Fer-RFP$^+$ rMSCs did and whether Ferucarbotran labeling could benefit the acquisition of functional differentiation of neuronal cells.

Although there are relatively few in vivo data on differentiation and functional incorporation of MSCs into host neurons after transplantation, our data highlight the need for in vivo model systems to assay MSCs' fates and biology in stroke. MSCs have been shown to exert their therapeutic benefits for stroke through multiple pathways as mentioned above; additionally, our recent study not only found bidirectional effects on proliferation between MSCs and the choroid plexus (CP) but also demonstrated the contributive role of these effects in MSCs' therapeutic benefits.[33] Moreover, our present study found that Ferucarbotran multifunctionally benefits MSCs' attributes to improve their therapeutic benefits. The combination of Ferucarbotran and MSCs may versatilely multiply MSCs' therapeutic benefits in many aspects.

Distribution and Survival of Fer-RFP$^+$ rMSCs

To evaluate the distribution, persistence, and viability of Fer-RFP$^+$ rMSCs following transplantation, in vivo MRI and histological analyses were performed 37 days after injecting 1×10^6 Fer-RFP$^+$ rMSCs into the caudate nucleus. As shown in Figure 6A, T2-weighted MRI revealed dark signal intensity regions corresponding to Fer-RFP$^+$ rMSCs. Guided by these MRI findings, tissues were collected from the corpus callosum, hippocampus, and third ventricle. Bright-field and

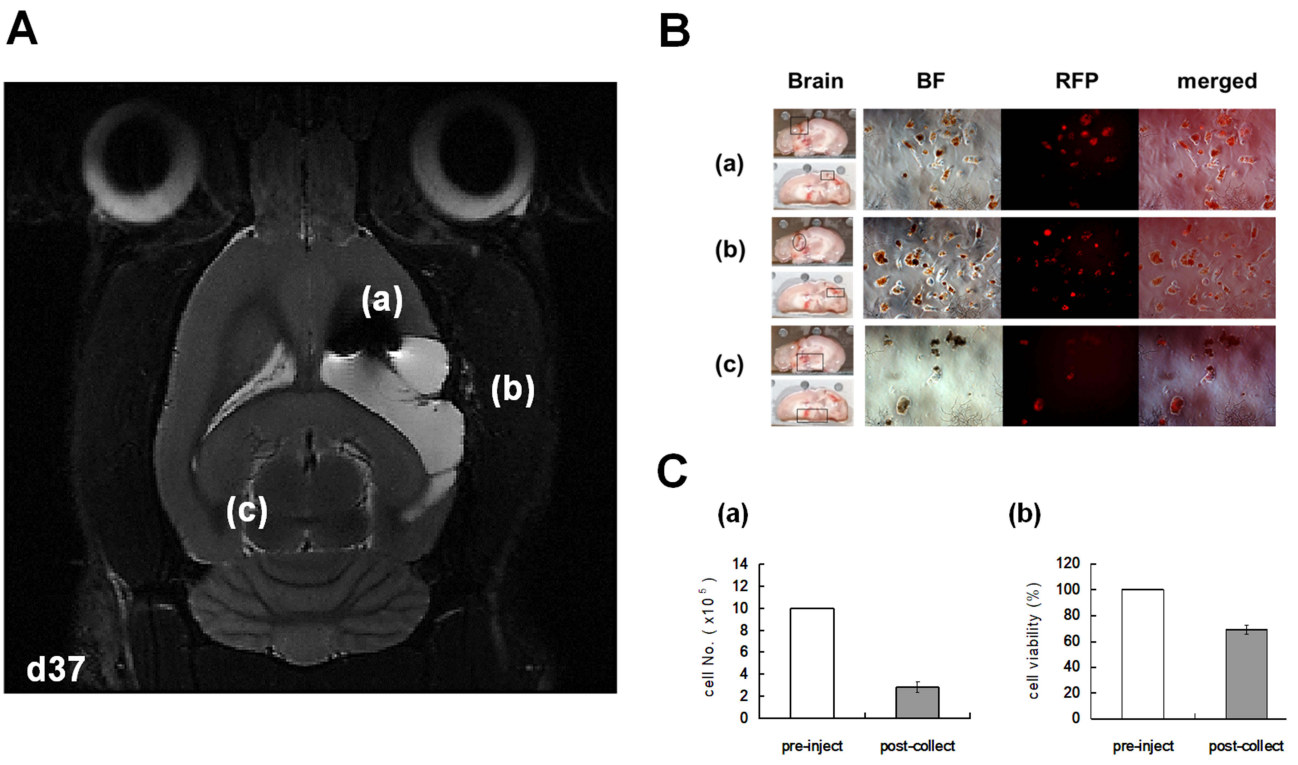

Figure 6 In vivo MRI and histological analyses were performed 37 days post-transplantation of 1 × 10^6 Fer-RFP$^+$ rMSCs into the caudate nucleus. (**A**) T2-weighted MRI showed dark signal intensity regions corresponding to Fer-RFP$^+$ rMSCs. (**B**) Bright-field and red fluorescence imaging confirmed viable Fer-RFP$^+$ rMSCs in the corpus callosum, hippocampus, and third ventricle. (Ca) Cell isolation from these regions recovered 2.85 × 10^5 Fer-RFP$^+$ rMSCs (~28.5% of injected cells), with 75% remaining viable in ex vivo culture (Cb).

https://doi.org/10.2147/IJN.S518933

red fluorescence imaging confirmed the presence of viable Fer-RFP$^+$ rMSCs within the brain parenchyma in these regions (Figure 6B).

To further quantify the retention of Fer-RFP$^+$ rMSCs, we isolated cells from the caudate nucleus, hippocampus, and third ventricle 37 days post-injection. Approximately 2.85×10^5 Fer-RFP$^+$ rMSCs were recovered, which is comparable to 28.5% of the originally injected 1×10^6 cells. Subsequent ex vivo culture revealed that ~75% of these isolated cells remained viable (Figure 6C).

Conclusion

We developed an MRI-based protocol to verify the biodistribution and migration of grafted rMSCs labeled with IONs, specifically Ferucarbotran, in an ischemic stroke model. Our results suggest that Ferucarbotran does not harm but instead benefits rMSCs' attributes, including proliferation, migration, and differentiation, for therapy in stroke. In addition to in vivo MRI, Ferucarbotran can be used for isolation of grafted rMSCs capable of differentiating into neuronal cells with functional activities, suggesting that the contribution of cell differentiation to stroke recovery warrants further study.

Abbreviations

MSCs, mesenchymal stem cells; MRI, magnetic resonance imaging; IONs, iron oxide nanoparticles; RFP, red fluorescent protein; hMSCs, human MSCs; rMSCs, rat MSCs; ROS, reactive oxygen species; MMP, mitochondrial membrane potential; SSC, side scatter counts; PB, Prussian blue; NeuN, neuronal nuclei; GFAP, glial fibrillary acidic protein; NESTIN, neuroepithelial stem cell protein. CC, Corpus Callosum.

Acknowledgments

We greatly appreciate technical support from the Core Laboratory of the Taipei Tzu Chi Hospital, Buddhist Tzu Chi Medical Foundation. The study was supported by grants from the Taipei Tzu Chi Hospital, Buddhist Tzu Chi Medical Foundation (TCRD-TPE-MOST-112-15, TCRD-TPE-112-04 and TCRD-TPE-NSTC-113-19) and National Science and Technology Council (National Science and Technology Council (NSTC 112-2321-B-002-024 and NSTC 113-2321-B-002-033), and the National Health Research Institutes (NHRI) (BN-113-PP-22 and BN-114-PP-22), Taiwan. We thank the excellent technical assistant of Instrumentation Center at NTU(Taiwan), Dr. Jyh-Horng Chen and Dr.Chao-Hsien Hsieh for MRI experiments.

Disclosure

The authors report no conflicts of interest in this work.

References

1. Feigin VL, Abajobir AA, Abate KH.; Group GBDNDC. Global, regional, and national burden of neurological disorders during 1990-2015: a systematic analysis for the global burden of disease study 2015. *Lancet Neurol*. 2017;16(11):877–897. doi:10.1016/S1474-4422(17)30299-5
2. Donnan GA, Fisher M, Macleod M, Davis SM. Stroke. *Lancet*. 2008;371(9624):1612–1623. doi:10.1016/S0140-6736(08)60694-7
3. Jingli Y, Jing W, Saeed Y. Ischemic brain stroke and mesenchymal stem cells: an overview of molecular mechanisms and therapeutic potential. *Stem Cells Int*. 2022;2022:5930244. doi:10.1155/2022/5930244
4. Hamblin MH, Lee JP. Neural stem cells for early ischemic stroke. *Int J Mol Sci*. 2021;22(14):7703. doi:10.3390/ijms22147703
5. Song CG, Zhang YZ, Wu HN, et al. Stem cells: a promising candidate to treat neurological disorders. *Neural Regen Res*. 2018;13(7):1294–1304. doi:10.4103/1673-5374.235085
6. Zhang S, Lachance BB, Moiz B, Jia X. Optimizing stem cell therapy after ischemic brain injury. *J Stroke*. 2020;22(3):286–305. doi:10.5853/jos.2019.03048
7. Gao Q, Wang L, Wang S, Huang B, Jing Y, Su J. Bone marrow mesenchymal stromal cells: identification, classification, and differentiation. *Front Cell Dev Biol*. 2021;9:787118. doi:10.3389/fcell.2021.787118
8. Steinberg GK, Kondziolka D, Wechsler LR, et al. Clinical outcomes of transplanted modified bone marrow-derived mesenchymal stem cells in stroke: a Phase 1/2a study. *Stroke*. 2016;47(7):1817–1824. doi:10.1161/STROKEAHA.116.012995
9. Wang F, Tang H, Zhu J, Zhang JH. Transplanting mesenchymal stem cells for treatment of ischemic stroke. *Cell Transplant*. 2018;27(12):1825–1834. doi:10.1177/0963689718795424
10. Eckert MA, Vu Q, Xie K, et al. Evidence for high translational potential of mesenchymal stromal cell therapy to improve recovery from ischemic stroke. *J Cereb Blood Flow Metab*. 2013;33(9):1322–1334. doi:10.1038/jcbfm.2013.91
11. Maria Ferri AL, Bersano A, Lisini D, Boncoraglio G, Frigerio S, Parati E. Mesenchymal stem cells for ischemic stroke: progress and possibilities. *Curr Med Chem*. 2016;23(16):1598–1608. doi:10.2174/0929867323666160222113702

12. Li Y, Chopp M. Marrow stromal cell transplantation in stroke and traumatic brain injury. *Neurosci Lett*. 2009;456(3):120–123. doi:10.1016/j.neulet.2008.03.096
13. Klein B, Ciesielska A, Losada PM, et al. Modified human mesenchymal stromal/stem cells restore cortical excitability after focal ischemic stroke in rats. *Mol Ther*. 2025;33(1):375–400. doi:10.1016/j.ymthe.2024.12.006
14. Borlongan CV. Concise review: stem cell therapy for stroke patients: are we there yet? *Stem Cells Transl Med*. 2019;8(9):983–988. doi:10.1002/sctm.19-0076
15. Steinberg GK, Kondziolka D, Wechsler LR, et al. Two-year safety and clinical outcomes in chronic ischemic stroke patients after implantation of modified bone marrow-derived mesenchymal stem cells (SB623): a phase 1/2a study. *J Neurosurg*. 2019;131(5):1462–1472. doi:10.3171/2018.5.JNS173147
16. Himmelreich U, Dresselaers T. Cell labeling and tracking for experimental models using magnetic resonance imaging. *Methods*. 2009;48(2):112–124. doi:10.1016/j.ymeth.2009.03.020
17. Hoehn M, Kustermann E, Blunk J, et al. Monitoring of implanted stem cell migration in vivo: a highly resolved in vivo magnetic resonance imaging investigation of experimental stroke in rat. *Proc Natl Acad Sci U S A*. 2002;99(25):16267–16272. doi:10.1073/pnas.242435499
18. Janowski M, Walczak P, Kropiwnicki T, et al. Long-term MRI cell tracking after intraventricular delivery in a patient with global cerebral ischemia and prospects for magnetic navigation of stem cells within the CSF. *PLoS One*. 2014;9(2):e97631. doi:10.1371/journal.pone.0097631
19. Ge J, Huang Z, Li C, et al. Magnetic resonance hypointensive signal primarily originates from extracellular iron particles in the long-term tracking of mesenchymal stem cells transplanted in the infarcted myocardium. *Int J Nanomed*;2015:1679. doi:10.2147/IJN.S77858
20. Terrovitis J, Stuber M, Youssef A, et al. Magnetic resonance imaging overestimates ferumoxide-labeled stem cell survival after transplantation in the heart. *Circulation*. 2008;117(12):1555–1562. doi:10.1161/CIRCULATIONAHA.107.732073
21. Winter EM, Hogers B, van der Graaf LM, Gittenberger-de Groot AC, Poelmann RE, van der Weerd L. Cell tracking using iron oxide fails to distinguish dead from living transplanted cells in the infarcted heart. *Magn Reson Med*. 2010;63(3):817–821. doi:10.1002/mrm.22094
22. Duan X, Lu L, Wang Y, et al. The long-term fate of mesenchymal stem cells labeled with magnetic resonance imaging-visible polymersomes in cerebral ischemia. *Int J Nanomed*. 2017;12:6705–6719. doi:10.2147/IJN.S146742
23. Zhou G, Wang Y, Gao S, et al. Potential mechanisms and perspectives in ischemic stroke treatment using stem cell therapies. *Front Cell Dev Biol*. 2021;9:646927. doi:10.3389/fcell.2021.646927
24. Liang L, Li Z, Ma T, et al. Transplantation of human placenta-derived mesenchymal stem cells alleviates critical limb ischemia in diabetic nude rats. *Cell Transplant*. 2017;26(1):45–61. doi:10.3727/096368916X692726
25. Agrawal H, Shang H, Sattah AP, Yang N, Peirce SM, Katz AJ. Human adipose-derived stromal/stem cells demonstrate short-lived persistence after implantation in both an immunocompetent and an immunocompromised murine model. *Stem Cell Res Ther*. 2014;5(6):142. doi:10.1186/scrt532
26. Oh SH, Choi C, Chang DJ, et al. Early neuroprotective effect with lack of long-term cell replacement effect on experimental stroke after intra-arterial transplantation of adipose-derived mesenchymal stromal cells. *Cytotherapy*. 2015;17(8):1090–1103. doi:10.1016/j.jcyt.2015.04.007
27. Han ZC, Du WJ, Han ZB, Liang L. New insights into the heterogeneity and functional diversity of human mesenchymal stem cells. *Bio-Med Mat Engineer*. 2017;28(s1):S29–S45. doi:10.3233/BME-171622
28. Shannon GS, Rinendyaputri R, Sunarno S, Malik A. Effects of stem cell therapy on preclinical stroke. *Open Vet J*. 2025;15(2):601–618. doi:10.5455/OVJ.2025.v15.i2.9
29. Chien LY, Hsiao JK, Hsu SC, et al. In vivo magnetic resonance imaging of cell tropism, trafficking mechanism, and therapeutic impact of human mesenchymal stem cells in a murine glioma model. *Biomaterials*. 2011;32(12):3275–3284. doi:10.1016/j.biomaterials.2011.01.042
30. Hsiao JK, Tai MF, Chu HH, et al. Magnetic nanoparticle labeling of mesenchymal stem cells without transfection agent: cellular behavior and capability of detection with clinical 1.5 T magnetic resonance at the single cell level. *Magn Reson Med*. 2007;58(4):717–724. doi:10.1002/mrm.21377
31. Lu CH, Hsiao JK. Diagnostic and therapeutic roles of iron oxide nanoparticles in biomedicine. *Tzu Chi Med J*. 2023;35(1):11–17. doi:10.4103/tcmj.tcmj_65_22
32. Lu CW, Hsiao JK, Liu HM, Wu CH. Characterization of an iron oxide nanoparticle labelling and MRI-based protocol for inducing human mesenchymal stem cells into neural-like cells. *Sci Rep*. 2017;7(1):3587. doi:10.1038/s41598-017-03863-x
33. Wu MR, Lee CH, Hsiao JK. Bidirectional enhancement of cell proliferation between iron oxide nanoparticle-labeled mesenchymal stem cells and choroid plexus in a cell-based therapy model of ischemic stroke. *Int J Nanomed*. 2020;15:9181–9195. doi:10.2147/IJN.S278687
34. Chung TH, Hsiao JK, Hsu SC, et al. Iron oxide nanoparticle-induced epidermal growth factor receptor expression in human stem cells for tumor therapy. *ACS Nano*. 2011;5(12):9807–9816. doi:10.1021/nn2033902
35. Huang DM, Hsiao JK, Chen YC, et al. The promotion of human mesenchymal stem cell proliferation by superparamagnetic iron oxide nanoparticles. *Biomaterials*. 2009;30(22):3645–3651. doi:10.1016/j.biomaterials.2009.03.032
36. Papanikolaou G, Pantopoulos K. Iron metabolism and toxicity. *Toxicol Appl Pharmacol*. 2005;202(2):199–211. doi:10.1016/j.taap.2004.06.021
37. Marchetti P, Castedo M, Susin SA, et al. Mitochondrial permeability transition is a central coordinating event of apoptosis. *J Exp Med*. 1996;184(3):1155–1160. doi:10.1084/jem.184.3.1155
38. Suski JM, Lebiedzinska M, Bonora M, Pinton P, Duszynski J, Wieckowski MR. Relation between mitochondrial membrane potential and ROS formation. *Methods Mol Biol*. 2012;810:183–205.
39. Chung TH, Hsu SC, Wu SH, et al. Dextran-coated iron oxide nanoparticle-improved therapeutic effects of human mesenchymal stem cells in a mouse model of Parkinson's disease. *Nanoscale*. 2018;10(6):2998–3007. doi:10.1039/C7NR06976F
40. Kubinova S. Biomaterials and magnetic stem cell delivery in the treatment of spinal cord injury. *Neurochem Res*. 2020;45(1):171–179. doi:10.1007/s11064-019-02808-2
41. Nishida K, Tanaka N, Nakanishi K, et al. Magnetic targeting of bone marrow stromal cells into spinal cord: through cerebrospinal fluid. *Neuroreport*. 2006;17(12):1269–1272. doi:10.1097/01.wnr.0000227993.07799.a2
42. Wilhelm C, Bal L, Smirnov P, et al. Magnetic control of vascular network formation with magnetically labeled endothelial progenitor cells. *Biomaterials*. 2007;28(26):3797–3806. doi:10.1016/j.biomaterials.2007.04.047
43. Pittenger MF, Discher DE, Peault BM, Phinney DG, Hare JM, Caplan AI. Mesenchymal stem cell perspective: cell biology to clinical progress. *NPJ Regen Med*. 2019;4(1):22. doi:10.1038/s41536-019-0083-6